

Article

Vadose Zone Transport of Tritium and Nitrate under Pondered Water Conditions

Philip H. Stauffer ^{*}, Brent D. Newman, Kay H. Birdsell, Marvin O. Gard, Jeffrey M. Heikoop, Emily C. Kluk and Terry A. Miller

Earth and Environmental Science Division, Los Alamos National Laboratory, Los Alamos, NM 87545, USA; bnewman@lanl.gov (B.D.N.); kay.birdsell@icloud.com (K.H.B.); mgard@lanl.gov (M.O.G.); jheikoop@lanl.gov (J.M.H.); lamkluk@aol.com (E.C.K.); tamiller@lanl.gov (T.A.M.)

* Correspondence: stauffer@lanl.gov; Tel.: +505-665-4638

Abstract: Vadose zone transport of tritium and nitrate can be important considerations at radioactive waste sites, landfills, or areas with industrial impacts. These contaminants are of particular concern because they typically have a relatively higher mobility in the subsurface compared to other compounds. Here, we describe a semiarid site with tritium and nitrate contamination involving a manmade ponded water source above a thick unsaturated zone at Los Alamos National Laboratory in New Mexico, USA. This study demonstrates the value of vadose zone flow and transport modeling for the development of field investigation plans (i.e., identifying optimal borehole locations and depths for contaminant characterization), and how a combination of modeling with isotope and geochemical measurements can provide insight into how tritium and nitrate transport in the vadose zone in semiarid environments. Modeling results suggest that at this location, tritium transport is well predicted by classical multiphase theory. Our work expands the demonstrated usefulness of a standard tritium conceptual model to sites with ponded surface conditions and agrees with previous results where a standard model was able to explain the evolution of a tritium plume at an arid waste disposal site. In addition, depth-based analyses of $\delta^{18}\text{O}$ and $\delta^2\text{H}$ of pore waters helped confirm the extent of pond infiltration into the vadose zone, and the $\delta^{15}\text{N}$ of nitrate showed that the contaminant release history of the site was different than originally assumed.

Keywords: vadose zone; stable isotope; tritium; contaminant transport



Citation: Stauffer, P.H.; Newman, B.D.; Birdsell, K.H.; Gard, M.O.; Heikoop, J.M.; Kluk, E.C.; Miller, T.A. Vadose Zone Transport of Tritium and Nitrate under Pondered Water Conditions. *Geosciences* **2022**, *12*, 294. <https://doi.org/10.3390/geosciences12080294>

Academic Editors: John M. (Jack) Sharp, Lhoussaine Bouchaou, Abdelfettah Sifeddine, Margaret A. Shanafield, Mohamed El-Alfy and Jesus Martinez-Frias

Received: 25 June 2022

Accepted: 25 July 2022

Published: 28 July 2022

Publisher's Note: MDPI stays neutral with regard to jurisdictional claims in published maps and institutional affiliations.



Copyright: © 2022 by the authors. Licensee MDPI, Basel, Switzerland. This article is an open access article distributed under the terms and conditions of the Creative Commons Attribution (CC BY) license (<https://creativecommons.org/licenses/by/4.0/>).

1. Introduction

Transport studies in the vadose zone cover a wide range of both natural and man-made chemical and isotopic signals. Such studies can benefit from a multi-tracer characterization approach, e.g., [1]. Tritium (^3H) is especially useful as a tracer of water movement due to its affinity for water molecules, thus traveling as tritiated water in both the liquid and vapor phases [2]. Although released in large quantities during atmospheric testing of nuclear weapons in the 1940s through 1963, tritiated water in the atmosphere has greatly decreased from a maximum concentration of greater than 10,000 pCi/L through both dilution and radioactive decay ($t_{1/2} = 12.3$ years), such that near-surface concentrations have returned to near pre-nuclear testing values of approximately 15–30 pCi/L [3,4]. Currently, tritium as hydrogen gas and tritiated wastewater, typically found at low-level radioactive waste disposal sites, nuclear test sites, and nuclear reactor facilities, has been demonstrated to be an effective indicator of contaminant migration [5,6]. With respect to health and safety, EPA guidance suggests a maximum contaminant level of 20,000 picocuries per liter (pCi/L) for tritium to remain below the dose-based drinking water standard of 4 mrem per year [7,8]. Tritium data collected in arid [6,9] and multiphase settings [10] have been used successfully in confirming conceptual models of transport through numerical simulation.

Stable isotopes of water (i.e., $\delta^{18}\text{O}$ and $\delta^2\text{H}$) are quite sensitive to phase changes such as evaporation [11,12]. Evaporation results in increases in stable isotope values that deviate from typical meteoric water values [11,13], thus making $\delta^{18}\text{O}$ and $\delta^2\text{H}$ useful tracers of percolation below features such as evaporation ponds. Characterization methods for measuring vadose zone $\delta^{18}\text{O}$ and $\delta^2\text{H}$ depth profiles are well established, e.g., [14–16], but underutilized. Nitrate stable isotopes ($\delta^{15}\text{N}$) can also be a useful tracer in contaminant studies because different nitrate sources can have different $\delta^{15}\text{N}$ values [11,13]. Thus, $\delta^{15}\text{N}$ values can provide a valuable source attribution tool, especially because many subsurface systems have measurable, and sometimes relatively large amounts of natural nitrate (e.g., [17]). In addition to isotopic tracers, major ion chemistry can also provide useful fingerprints of vadose-zone flow and transport. Anions such as bromide, chloride, nitrate, and sulfate are particularly useful because they are often quite mobile compared to most cations.

In the work presented here, we use a combination of these tracers to better understand the flow and transport from evaporative surface impoundments at Los Alamos National Laboratory (LANL) in New Mexico, USA. We summarize the analysis of the transport of water, and the chemical and isotopic signatures beneath the TA-53 surface impoundments. The objective of this study is to interpret stable isotope ($\delta^{18}\text{O}$, $\delta^2\text{H}$, and $\delta^{15}\text{N}$), anion, tritium, and moisture profiles from cores retrieved from the deepest borehole at the site in terms of past hydrologic behavior and contaminant extent beneath the surface impoundments. A second goal is to determine what portion of the site was impacted by leakage from surface releases. Because the water in the impoundments was subject to substantial evaporation, which affects the stable isotope values, it is hypothesized that the $\delta^{18}\text{O}$ and $\delta^2\text{H}$ data could indicate how the effluent water has moved downward in the mesa. It was also hypothesized that the anion data may indicate the depth of movement of impounded water. Further, the presence of tritium further indicates migration from the impoundments to depth. The tritium data are used to constrain simulations of tritium transport in the subsurface. The simulations create a bounding case scenario of water and tritium migration beneath the impoundments. Simulations are presented to show that the most recent observations of tritium and water saturation beneath the impoundments can be explained within the framework of a standard tritium transport conceptual model. These results advance the work of Maples et al. [6] and Garcia et al. [9] by including a ponded source region that complicates the tritium migration. Further, the data and modeling results provide a useful reference case for understanding unsaturated zone flow and contaminant transport in dryland environments with thick vadose zones and are relevant to other studies where flow and transport from ponded industrial water sources may be important.

2. Materials and Methods

2.1. Site Description

Three surface impoundments that were built to evaporate effluent from Technical Area 53 (TA-53) at LANL are the focus of this study. The main activity of TA-53 centers around the Los Alamos Neutron Science Center (LANSCE) and associated experimental facilities. LANSCE produces intense ion beams from an 800-mega-electron-volt linear accelerator [18]. During the time that the surface impoundments were used, activities at TA-53 focused on medium energy physics research. Radioactive liquid waste streams from the accelerator facility included tritium and other short-lived radionuclides.

The surface impoundments are located on the Pajarito Plateau on the eastern flank of the Jemez Mountains in northern New Mexico (Figure 1. [19]). The plateau is composed of finger mesas with deep canyons carved into the rocks of the Bandelier Tuff over the last 1.6 M years [20]. The two northern surface impoundments were designed to hold 12,100 m³ wastewater from various TA-53 facilities. The northern impoundments were constructed in 1969 by excavating into the tuff and placing a clay liner on the surface of the tuff. Gunite (concrete) was sprayed onto the crushed tuff berm. The two impoundments originally were planned as wastewater retention surface impoundments. The surface impoundments

received a variety of wastewater from various TA-53 facilities, including sanitary and radioactive liquid wastewater from lines serving 420 structures. Thirty meters south of the center of the northern impoundments, an unlined overflow drainage was cut into the tuff and flowed east, draining over the edge of the mesa into a tributary of Los Alamos Canyon (pink circles, inset of Figure 1). This drainage ditch was removed in 1985 during construction of the southern impoundment [21–23].

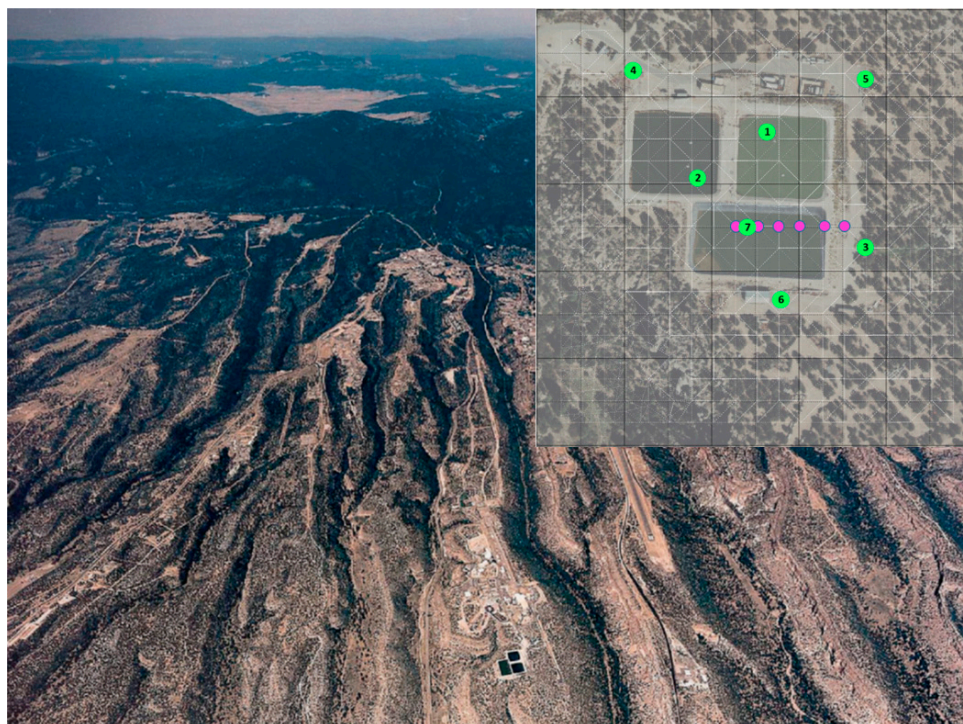


Figure 1. Aerial photograph of Los Alamos and the Pajarito Plateau looking west into the Jemez Mountains. The surface impoundments of TA-53, prior to remediation, are visible in the bottom middle of the figure (after Newman and Robinson, 2005). The inset shows the locations of the seven monitoring boreholes drilled in 2002 (green numbered circles) and the approximate trajectory of the unlined drainage ditch (pink circles).

The southern surface impoundment was constructed in 1985 by excavating into tuff, overlaying the exposed tuff with crushed tuff and sand, and covering with a Hypalon™ (rubber polymer) liner. The original purpose of the southern impoundment was to receive overflow from the two northern impoundments, but starting in 1989, this impoundment became the primary recipient of radiological waste, while sanitary waste was diverted solely to the northern impoundments. From 1985 to 1992, occasional releases from the northern impoundments occurred through an overflow pipe leading off the mesa. Starting in 1992, the LANL Sanitary Wastewater System Consolidation (SWSC) became operational, and all sanitary waste was diverted from the northern surface impoundments to the SWSC. The southern impoundment continued to receive radiological waste until 1998 with no reported overflows in the period of 1989–1998 [21–23].

The surface impoundments were remediated in the early 2000s as part of the U.S. Resource Conservation and Recovery Act (RCRA) corrective actions. Shallow boreholes drilled during remediation activities showed concentrations of tritium, nitrate, and other constituents to depths of 30 m, with the highest concentrations of tritium reaching 100 nCi/L at 30 m below the impoundment surface [23]. The primary contaminant of concern at this site is tritium. The water table is deep relative to the plume at approximately 300 m depth, so the contaminants remain well within the vadose zone.

As part of the corrective action at this site, LANL was directed to define the nature and extent of any contamination resulting from leakage out of the surface impoundments. After removal of the surface impoundments in 2000–2002, seven new boreholes were drilled to define the nature and extent of the contaminants in the upper vadose zone (inset to Figure 1). The vertical extent of the plume is based on borehole 53-02-20824 (hereafter referred to as Borehole 7). Borehole 7 was drilled at the northern edge of the footprint of the southern impoundment. This borehole was drilled at the approximate centroid of the three TA-53 surface impoundments, close to the unlined drainage ditch, and provides a representation of the TA-53 subsurface [23].

2.2. Conceptual Model of Transport beneath the TA-53 Surface Impoundments and Drainage Ditch

Our conceptual model of transport in the dry mesa underlying the TA-53 impoundments is summarized as follows. Liquid effluent, mainly water containing some contamination, has infiltrated the dry rock beneath the impoundments primarily through the drainage ditch and is moving under the forces of gravity and capillary suction. Gravity pulls water down while capillary suction pulls water from areas of high saturation to areas of low saturation. During the period of active infiltration from the surface, high saturations allowed liquid water to move more quickly to depth. Since the effluent source was removed, capillary forces continue to spread the subsurface effluent into regions of lower saturation leading to a much slower liquid flow rate. As liquid flow is reduced, vapor transport in the vadose zone becomes more important [24,25]. Our conceptual model of transport is based on decades of research and local field observations [26–28]. Model calibration of field injection experiments in boreholes within the vadose zone and from waste infiltration galleries have verified our ability to use standard unsaturated zone flow theory to implement the conceptual model in a numerical framework [24,29].

For tritium transport, our conceptual model of release from the wet surface impoundments and transport through the dry host rock assumes that the majority of tritium was released in the form of liquid water and that each tritium atom is attached singly to a water molecule [30]. Tritium is radioactive hydrogen with a half-life of 12.3 years. It is incorporated into the water molecule to form a tritiated water molecule (sometimes called HTO) that behaves nearly identically to normal water with respect to transport in the environment. Being intimately bound to water, tritium migrates as both liquid water and as water vapor in the pore gas (soil air) [31].

Within the unsaturated porous media, equilibrium between water and water vapor is assumed (a well-mixed model) because diffusive transport of both phases is slow relative to the rate of tritium exchange between pore water and pore gas [32]. Tritium in the vapor phase equilibrates with residual liquid pore water before diffusing through the air-filled pore space [32]. Migration of tritium due to water vapor transport is important in arid and semiarid regions with low moisture content such as at this LANL site. Vapor transport becomes the dominant transport mechanism as the liquid effluent is spread by capillary suction after the source is removed [27,29]. Finally, the short half-life of tritium causes a large reduction in the inventory during the time needed to migrate from the source.

2.3. Field Methods

Core was collected from a hollow-stem auger system during the drilling of Borehole 7 and analyzed for anion concentrations using a leaching process previously described by [16]. The analytical suite included bromide, chloride, chlorate, fluoride, nitrate, nitrite, phosphate, oxalate, and sulfate. Moisture-protected core samples were collected and analyzed between 3.2- and 86.7-m depths. The stratigraphic units sampled include (from bottom to top) the Otowi member of the Bandelier Tuff, the Cerro Toledo Formation, the Tsankawi Pumice, and Tshirege member units 1g, 1v, and 2 of the Bandelier Tuff.

Pore water anion concentrations were calculated from dried samples of core using leachate concentrations (measured using ion chromatography), gravimetric water contents (measured using ASTM method D2216-90), and bulk densities. Bulk density was not

measured on the samples; therefore, typical local Los Alamos bulk density measurements for the specific tuff and pumice units encountered in the borehole were used [33].

Stable isotope analyses ($\delta^{18}\text{O}$ and $\delta^2\text{H}$) were also performed on water samples extracted from moisture-protected cores. These analyses provide data on the isotopic composition of the pore water and are an effective way of characterizing hydrologic processes in semiarid environments such as the Pajarito Plateau. Analyses for $\delta^{18}\text{O}$ and $\delta^2\text{H}$ of core pore waters were performed at the Stable Isotope Laboratory at the New Mexico Institute of Mining and Technology. The sample preparation for $\delta^{18}\text{O}$ and $\delta^2\text{H}$ analyses was previously described in Newman et al. (2010) and used the vacuum distillation method of Shurbaji and Campbell [34], and the $\delta^{18}\text{O}$ and $\delta^2\text{H}$ extraction methods of Socki et al. [35] and Kendall and Coplen [36], respectively. The analytical precision for the $\delta^{18}\text{O}$ and $\delta^2\text{H}$ analyses by mass spectroscopy was better than $\pm 0.2\text{‰}$ and $\pm 4\text{‰}$, respectively. The hydrogen and oxygen isotopes are reported in delta (δ) notation as permil (‰) differences relative to the Vienna Standard Mean Ocean Water (V-SMOW) isotope standard:

$$\delta^2\text{H or } \delta^{18}\text{O} = \left[\frac{R_{\text{sample}} - R_{\text{V-SMOW}}}{R_{\text{V-SMOW}}} \right] \times 1000 \quad (1)$$

where R is the $^2\text{H}/^1\text{H}$ or $^{18}\text{O}/^{16}\text{O}$ ratio. Because the V-SMOW standard has a relatively large heavy to light isotope ratio ($R_{\text{V-SMOW}}$), negative delta values are commonly observed for precipitation, surface water, and ground water.

In addition to the pore water isotope analyses, an additional set of core leaches was conducted to collect nitrate for nitrogen-stable isotope analyses ($\delta^{15}\text{N}$). Nitrogen isotopes can be an effective indicator of the source of nitrogen (or nitrate) in the environment (e.g., whether the nitrate had a natural or anthropogenic source). The leaching was performed on remnant core samples after the anion leaching was completed. Nitrate leaching followed the same procedure as the anions, except that approximately 1 kg of sample was leached with 1.5 L of water to recover enough nitrate for the analysis. Only a limited set of samples was leached and analyzed, mainly because nitrate concentrations were not high enough in some samples to perform the isotopic analysis. Recovery of the nitrate from the sample leachates and the $\delta^{15}\text{N}$ isotope analysis method were conducted following Chang et al. [37] and Silva et al. [38]. The $\delta^{15}\text{N}$ results are reported in delta (δ) notation as ‰ differences relative to the atmospheric nitrogen (AIR) standard. The analytical precision of the mass spectrometer $\delta^{15}\text{N}$ results is better than 1‰.

Tritium analyses were conducted on waters extracted from moisture-protected core samples collected during hollow stem auger drilling. Samples were analyzed using liquid scintillation counting and details are provided in LANL [23].

2.4. Numerical Model of Tritium Transport

A site-specific, three-dimensional tritium transport model was originally developed to support decisions regarding borehole placement for determining the maximum horizontal and lateral extent of tritium beneath the TA-53 surface impoundments [39]. The same numerical model is used in the current analysis to bound future tritium transport. The simulations are run using FEHM [40–42]. FEHM is regularly benchmarked against an extensive test suite to ensure continued adherence to analytical and semi-analytical flow and transport solutions [42]). This project led to the creation of a new analytical test problem related to tritium transport that is described in detail below. Publications illustrating other transport models using FEHM include contributions to the Yucca Mountain Project [43–45] and LANL site environmental analysis [24–26,28,29,46–48].

The conceptual model of dual-phase tritium transport was simulated using an equivalent, enhanced, liquid-phase, diffusion coefficient formulation. The Smiles formulation [32] relates effective diffusion (D_{eff}) in a single phase to the full two-phase formulation as:

$$D_{\text{eff}} = H \frac{\theta_a}{\theta_w} D_a + D_w \quad (2)$$

where H is the dimensionless Henry's partitioning factor, θ_a and θ_w are air and water volume fraction of the total rock volume (air and water content), and D_a and D_w are the molecular diffusion coefficients in the vapor and liquid phases of the rock, modified for tortuosity [42]. Water content can be defined as saturation (s) multiplied by porosity (φ), while air content is defined as $(1-s)$ multiplied by φ . The ability to represent two-phase flow and transport using the Smiles formulation is demonstrated in Figure 2 using two parameter sets within FEHM. These code verification simulations use a 1-D numerical mesh of 10-m length with a node spacing of 0.2 m. Concentration results are shown for a point 5 m from a fixed concentration of 1 mol (tritium) per kg of water using both the single-phase [32] formulation and a full multiphase solution. Case one in Figure 2 uses a saturation of 0.01, a porosity of 0.2, a D_w of 1×10^{-9} m²/s, and a $D_a = 1 \times 10^{-5}$ m²/s, yielding a D_{eff} of 1.8×10^{-8} m²/s. Case two in Figure 2 uses a saturation of 0.2, a porosity of 0.5, a D_w of 1×10^{-10} m²/s, and a $D_a = 1 \times 10^{-4}$ m²/s, yielding a D_{eff} of 6.9×10^{-9} m²/s. Although FEHM is capable of simulating full multiphase, thermally driven, tritium transport [49], the decision to use the simplified, single-phase representation of tritium transport at this site was based on the low thermal gradient (i.e., nearly isothermal conditions). These two examples verify that the single-phase formulation is accurate as implemented in FEHM.

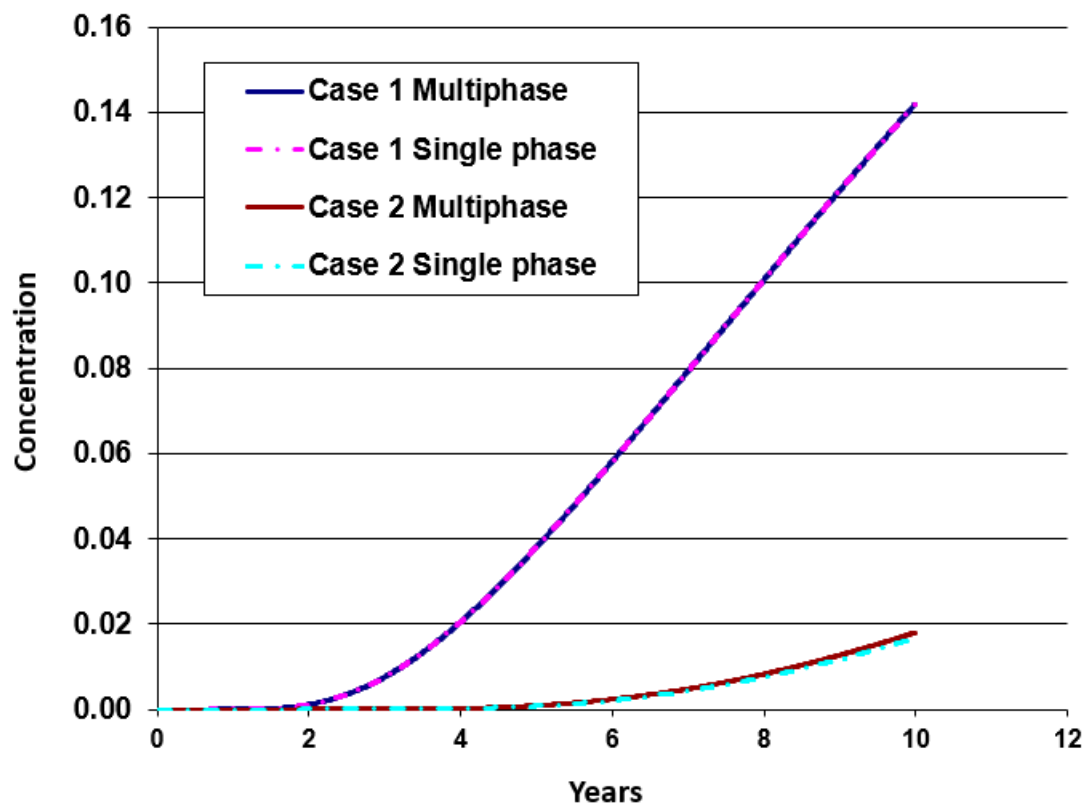


Figure 2. Comparison of two-phase tritium transport to the Smiles et al. (1995) [32] single-phase equivalent formulation, all simulations run with FEHM.

Site-specific geologic and hydrologic data [24–26] were used to develop a numerical mesh from the land surface to the water table that encompasses a lateral area centered on the impoundments (Figure 3). Geological units shown on this figure, starting at depth and moving upward, include the Puye Formation (loosely consolidated sands and gravels), the Cerros del Rio basalt (interbedded massive and rubble zones), the Guaje Pumice (the basal ash flow of the Bandelier Tuff), the Otowi member of the Bandelier Tuff (Qbo), a volcanoclastic sedimentary unit (Qct or the Cerro Toledo interval), and finally the Tshirge member of the Bandelier Tuff comprised of the basal Tsankawi Pumice (Qtsk), and overlying

units Qbt1g, Qbt1v, and Qbt2. These rocks range in age from 1.2 Ma on the surface to Pliocene age rocks greater than 2.5 Ma in the Puye formation [20].

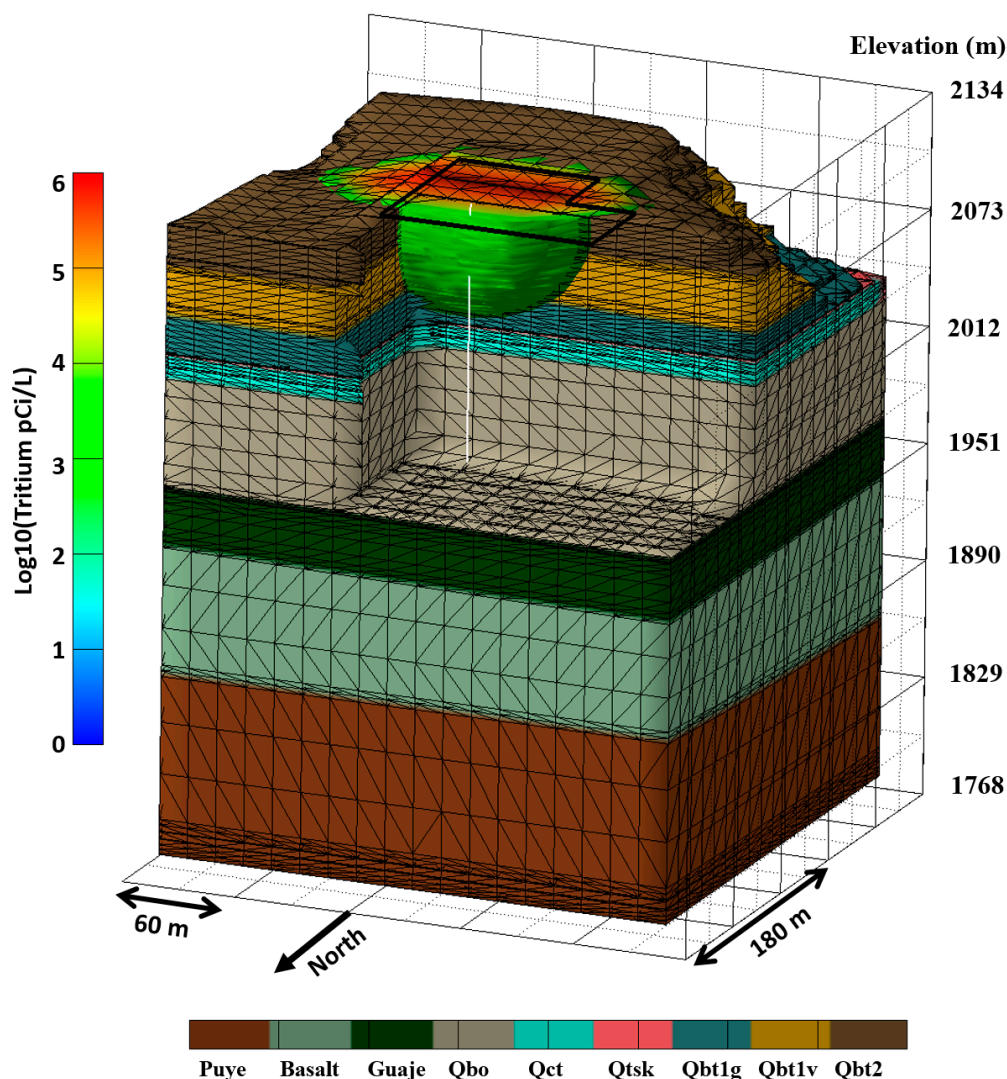


Figure 3. Three-dimensional numerical mesh used for all tritium simulations. Color contours show the year 2002 simulated extent of the 1000 pCi/L tritium plume for the bounding case. Geologic unit abbreviations are described in the text.

The numerical mesh was generated using LaGrit grid generation software [50] and incorporates information from the LANL site-wide geologic model. Hydrogeologic properties including porosity, permeability, and Van Genuchten retention parameters [24–26] are assigned to the different geologic units shown in Figure 3 [51]. Finite volume elements are 15.24 m in both x and y, while vertical spacing varies to capture thinner geologic units and unit interfaces as seen in Figure 3. A more complete description of the mesh generation process can be found in Miller et al. [52]. Hydrological values for these rocks, including all van Genuchten parameters, and a description of the underlying unsaturated flow equations can be found in Stauffer et al. [24] and Stauffer et al., [53], respectively and are reproduced here in Table 1. The land surface boundary is fixed to zero concentration of tritium, while the lateral boundaries of the model are no-flow. The bottom boundary is a drainage condition to allow excess water to flow out of the domain with little resistance. A combined effective diffusion coefficient [32] of $1.53 \times 10^{-8} \text{ m}^2/\text{s}$ was used, and the simulations were found to be insensitive to this parameter because the primary transport mechanism is advective liquid flow. Initial tritium concentration in the subsurface is set to zero.

Table 1. Hydrogeologic properties used for the three-dimensional model.

Geologic Unit	Bulk Density (kg/m ³)	Permeability (m ²)		ϕ	Van Genuchten Parameters		
		Horiz.	Vert.		Sat_{res}	α (1/m)	n
Tshirege Qbt2	1.6×10^3	1.2×10^{-13}	1.2×10^{-13}	0.40	0.017	0.30	2.2
Tshirege Qbt1v	1.3×10^3	5.1×10^{-13}	5.1×10^{-13}	0.51	0.004	0.54	1.7
Tshirege Qbt1g	1.2×10^3	6.8×10^{-13}	6.8×10^{-13}	0.56	0.00	0.63	1.6
Tsankawi Pumice	ND	2.2×10^{-12}	2.2×10^{-12}	0.59	0.00	0.43	1.9
Cerro Toledo interval	1.2×10^3	7.1×10^{-13}	7.1×10^{-13}	0.51	0.00	0.53	1.4
Otowi	1.2×10^3	9.8×10^{-14}	9.8×10^{-14}	0.53	0.008	0.30	2.0
Guaje Pumice	8.4×10^2	1.6×10^{-13}	1.6×10^{-13}	0.66	0.00	0.28	2.5
Cerros del Rio basalt	ND	1.0×10^{-12}	1.0×10^{-12}	0.001	0.001	3.8	1.5
Puye Formation	2.6×10^3	8.7×10^{-13}	4.1×10^{-14}	0.21/0.40	0.0012	0.85	2.3

Numbers are rounded to two significant digits, NA = Not applicable, ND = No data.

The simulations are run for a period of 100 years. The first 15 years (1970–1985) represent the active “wet” leaking phase at the site with enhanced infiltration and high tritium concentrations in the effluent. The final 85 years represent the period after removal of the effluent source (and the overflow drainage ditch). Site data on water discharge to the drainage ditch from the TA-53 surface impoundments are available for the years 1978 to 1989 [21]. Focusing on the existing data through 1985 when the unlined drainage ditch was being used, we calculate an order of 2×10^7 L/year were discharged. Extrapolating for the entire 15 years of operations of the unlined drainage ditch yields an estimate of 3×10^8 L of total discharge. An estimate of source concentration was developed by decay correcting the highest measured 2002 near surface concentration back to a 1985 value of 1.43×10^6 pCi/L. In the absence of other data, the estimated source concentration in the injected water was applied to all infiltrated effluent. To estimate the maximum amount of effluent that infiltrated the unlined drainage ditch, we use the numerical model to vary infiltration flux until subsurface concentrations in the simulation bound the data.

3. Results

3.1. Field/Core Analysis Results

3.1.1. Moisture Content and Tritium Data from Borehole 7

Moisture content and tritium data from Borehole 7 are shown in Table 2. Water content values range from 3–20% gravimetric moisture and are well below saturation. Tritium soil concentrations ranged from below detection to just over 30 pCi/gram of soil. Soil concentrations were highest in the shallowest depths and were below detection at depths greater than 46 m. Table 2 also shows soil concentrations converted to pore water concentration units used to compare data to simulation results. Water content (θ_w), in this case, is defined as the mass of water divided by the mass of solid material, and is converted to saturation using the following easily derived relationship:

$$s = \theta_w \frac{2.65 \cdot (1 - \phi)}{\phi} \quad (3)$$

where ϕ is porosity and the assumed grain density of the tuff units is 2650 kg/m³. Porosity values are listed in Table 2 and come from Stauffer et al. [24]. Conversion of pCi per wet gram to pCi per liter follows a similar approach. Skipping the derivation, we arrive at:

$$\frac{\text{pCi}}{\text{L}} = 1000 \cdot \left(\frac{\text{pCi}}{\text{g}} \text{wet} \right) \cdot \frac{2.65 \cdot (1 - \phi) + \phi s}{\phi s} \quad (4)$$

where the factor of 1000 converts from cm³ of water to liters of water.

Table 2. Borehole 7 moisture content, saturation, porosity and tritium concentration data.

Depth (m)	Percent Moisture (θ_w)	pCi/g Wet	Porosity	Saturation (s)	pCi/L
3.2	6.1	31.7	0.4	0.24	551,372
6.1	5.9	13.5	0.4	0.23	242,314
9.1	5.1	20.4	0.4	0.20	420,400
12.2	4.3	19.7	0.4	0.17	477,840
15.2	4	11.9	0.4	0.16	309,400
18.3	3.4	9.99	0.4	0.14	303,814
21.3	5	10.1	0.4	0.20	212,100
24.4	6.3	11.6	0.4	0.25	195,727
27.4	6.3	11.6	0.4	0.25	195,727
30.5	7	11.6	0.4	0.28	177,314
33.5	6.2	11	0.51	0.16	188,419
36.6	9.6	10.4	0.51	0.24	118,733
39.6	10.9	7.25	0.51	0.28	73,764
42.7	13.6	1.45	0.51	0.35	12,112
45.7	17.2	0.17	0.56	0.36	1158
48.8	12.3	0.077	0.56	0.26	703
51.8	10.7	−0.065	0.56	0.22	BD
54.9	11.2	0.085	0.56	0.23	844
57.9	12.5	−0.038	0.56	0.26	BD
61.0	12.8	−0.091	0.56	0.27	BD
64.0	11	−0.128	0.56	0.23	BD
66.9	10.6	0.07	0.56	0.22	730
69.8	11	−0.116	0.56	0.23	BD
73.0	12.5	−0.122	0.56	0.26	BD
74.3	17	−0.1	0.59	0.31	BD
77.6	6.6	−0.085	0.51	0.17	BD
80.5	5.6	0.169	0.51	0.14	3187
83.7	5.3	0.22	0.51	0.13	4371
86.5	6.3	0.115	0.53	0.15	1940
90.9	5.9	0.014	0.53	0.14	251

BD—below detection.

3.1.2. Anion Profiles from Borehole 7

The vertical distributions of bromide, chloride, fluoride, nitrate (as nitrate), nitrite (as nitrite), oxalate, phosphate, and sulfate pore water concentrations from core samples collected from Borehole 7 are shown in Table 3 and are plotted in Figures 4 and 5. Anions with maximum concentrations less than 10 mg/L are shown in Figure 4, and anions with maximum concentrations greater than 10 mg/L are shown in Figure 5.

Table 3. Borehole 7 pore water anion concentrations.

Depth (m)	Grav. Water (%)	Br ⁻ (mg/L)	Cl ⁻ (mg/L)	F (mg/L)	NO ₂ ⁻ (mg/L)	NO ₃ ⁻ (mg/L)	Oxalate (mg/L)	PO ₄ ⁻ (mg/L)	SO ₄ ⁻ (mg/L)
3.2	5	3.8	146	61	BD	6.0	5.8	0.82	310
9.4	4	4.5	173	115	BD	1.5	2.3	6.8	32
15.5	4	6.0	166	186	0.4	1.1	0.7	2.5	21
21.5	3	8.2	202	230	BD	0.5	BD	5.3	14
27.6	6	4.3	128	108	0.3	6.3	BD	1.8	17
33.7	8	2.3	109	73	BD	14	BD	0.75	22
39.8	10	2.3	79	58	BD	11	BD	0.57	20
45.9	20	2.4	49	32	0.2	13	BD	0.15	199
52.0	12	2.4	101	31	0.1	19	BD	0.26	75
58.1	15	2.1	50	34	BD	1.8	BD	0.10	37
64.2	13	2.3	48	39	0.1	0.9	0.2	0.23	42
70.0	13	1.9	46	41	0.1	2.6	0.4	0.24	11
74.5	20	0.7	36	28	BD	1.6	BD	0.23	12
80.6	7	3.6	59	59	BD	BD	0.64	0.64	6.6
86.7	7	3.3	66	41	0.2	2.9	0.6	1.0	4.2

Anions whose concentrations fell below the detection limit are reported as below detection (BD) in Table 3. To construct the figures presented in this report a value of 0 was used for the BD values.

3.1.3. Stable Isotope Profiles from Borehole 7

The $\delta^{18}\text{O}$ and $\delta^2\text{H}$ profiles from the Borehole 7 core show large isotopic values from approximately 3- to approximately 40-m depths (Table 4, Figure 6). At depths between approximately 40- and 57-m, $\delta^{18}\text{O}$ and $\delta^2\text{H}$ values decrease substantially. At depths below about 57 m, the stable isotope values decrease, but less dramatically than in the 40- to 57-m zone.

Table 4. Borehole 7 (53-20824) stable isotope values.

Depth (m)	$\delta^{18}\text{O}$ (‰)	$\delta^2\text{H}$ (‰)	$\delta^{15}\text{N}$ (‰)
3.2	-4.2	-49	15.9
9.4	-3.4	-44	12.9
15.5	-2.8	-47	NA
21.5	-2.1	-45	NA
27.6	-2.5	-44	12.7
33.7	-1.9	-40	17.4
39.8	-2.4	-41	13.6

Table 4. Cont.

Depth (m)	$\delta^{18}\text{O}$ (‰)	$\delta^2\text{H}$ (‰)	$\delta^{15}\text{N}$ (‰)
45.9	−5.9	−59	16.9
52.0	−8.6	−79	9
58.1	−11.5	−93	10
64.2	−11.5	−98	NA
70.0	−11.5	−102	7.7
74.5	−13.4	−105	11
80.6	−12.0	−106	NA
86.7	−12.7	−107	NA

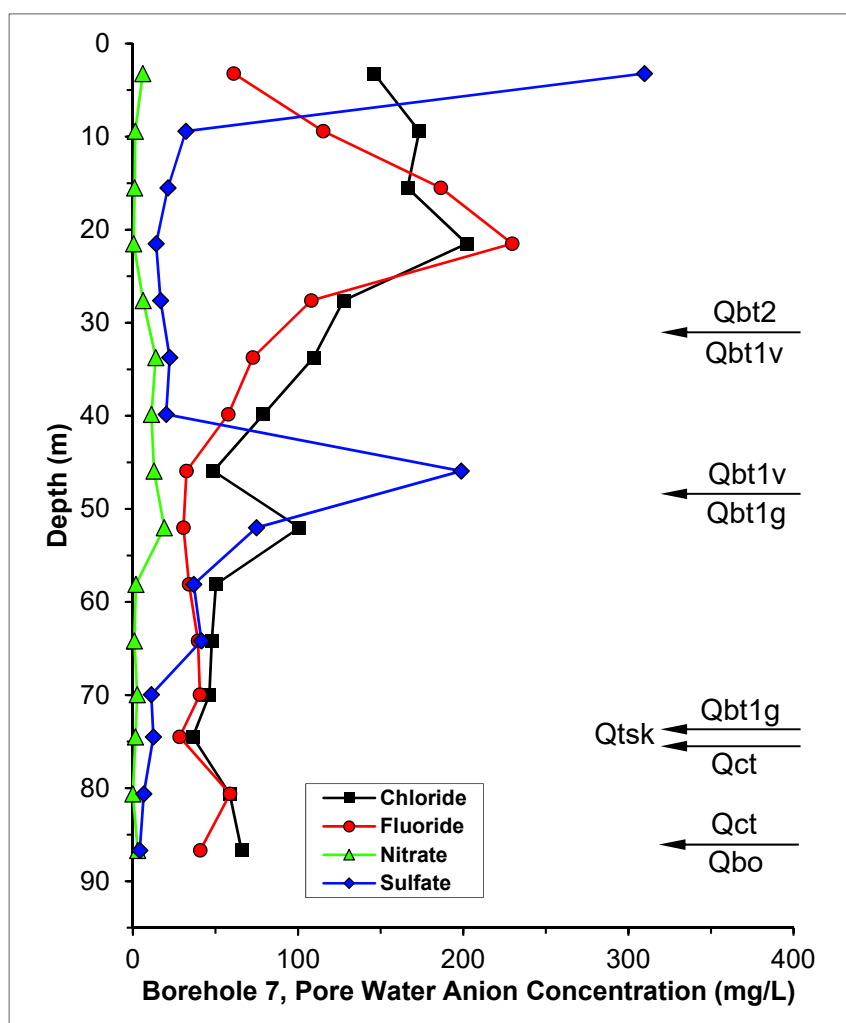


Figure 4. Pore waterpr chloride, fluoride, nitrate, and sulfate concentrations in Borehole 7, TA-53. Stratigraphic contacts are shown on the right side of the figure.

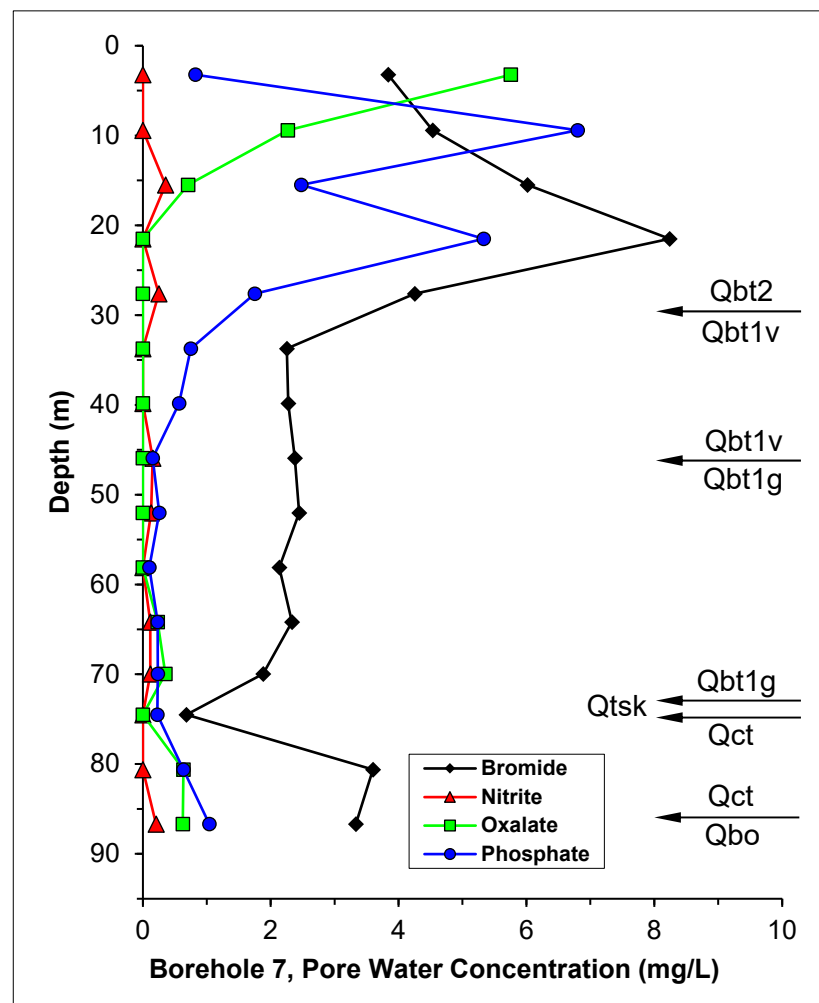


Figure 5. Pore water bromide, nitrite, oxalate, and phosphate concentrations in Borehole 7, TA-53. Stratigraphic contacts are shown on the right side of the figure.

The $\delta^{15}\text{N}$ data show positive values throughout the profile and range from 7.7 to 17.4‰ (Table 4). The highest values occur in the upper 45 m of the profile.

3.2. Bounding Case Simulation Results

Simulation results presented are for the bounding case derived from our sensitivity analysis. A limited number of simulations were performed to determine if leakage through the unlined drainage ditch could be adjusted within the bounds of the conceptual model to explain the depth of observed tritium, particularly in Borehole 7. The location of the seven boreholes drilled in 2002 are shown in Figure 7. These boreholes were drilled to delineate the extent of the tritium plume. The lateral extent of the numerical grid used to calculate tritium transport and changes in saturation is also shown in Figure 7. Water injection locations (pink circles) representing the unlined drainage ditch are also shown.

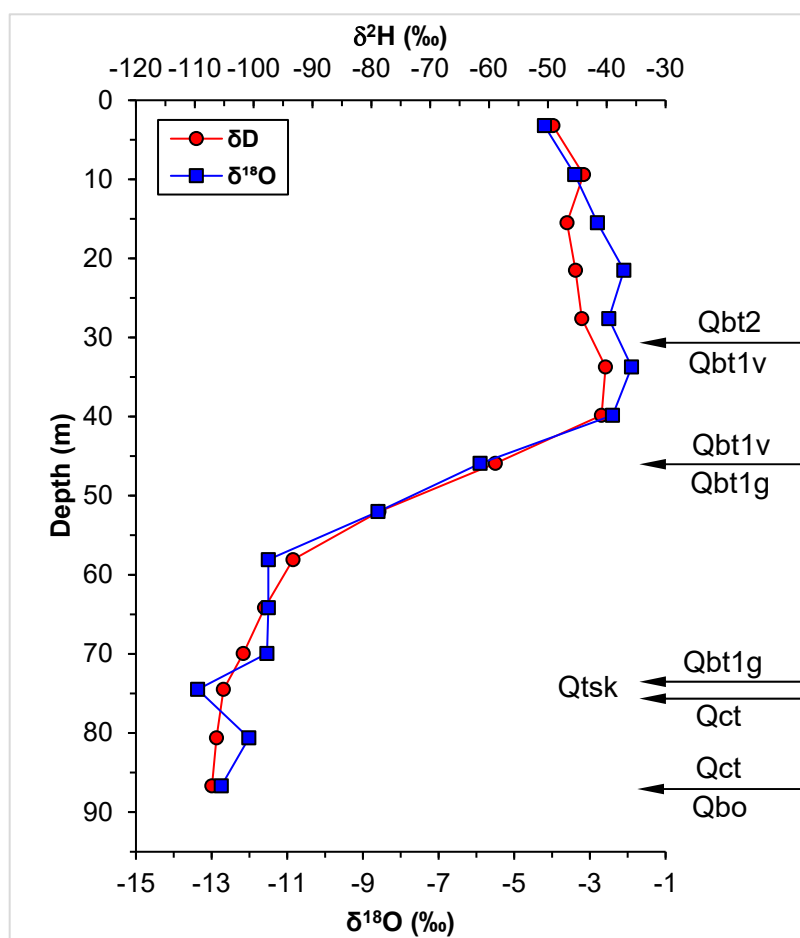


Figure 6. Stable isotope ($\delta^{18}\text{O}$ and $\delta^2\text{H}$) profiles in Borehole 7, TA-53. Stratigraphic contacts are shown on the right side of the Figure.

The simulations were initiated by running the flow simulation to a steady state using a 1 mm/year (1 L per m^2 per year) background infiltration flux across the upper boundary. This minimal flux was not applied during the years of 1970–2001, during which time most of the site was covered with impermeable liners (clay/HypalonTM). In 2002, after site remediation, background infiltration was reset to 1 mm/year through the year 2070.

The only parameter that was varied (manually) to generate a bounding case is the volume of infiltration flux during the active period. The bounding case has enhanced infiltration from leakage, used to simulate the active wet period of operation, of 1 m^3 per m^2 /year over an area of 1394 m^2 . This area aligns with where the unlined outfall channel was located. The bounding case of simulated leakage injection is equal to a volume of 1394 m^3 /year. The total volume of the simulated infiltration from the unlined drainage ditch over the 15-year period, $2.1 \times 10^4 \text{ m}^3$, represents a significant fraction (7%) of the total estimated discharge from the impoundments to the drainage ditch ($3.0 \times 10^5 \text{ m}^3$).

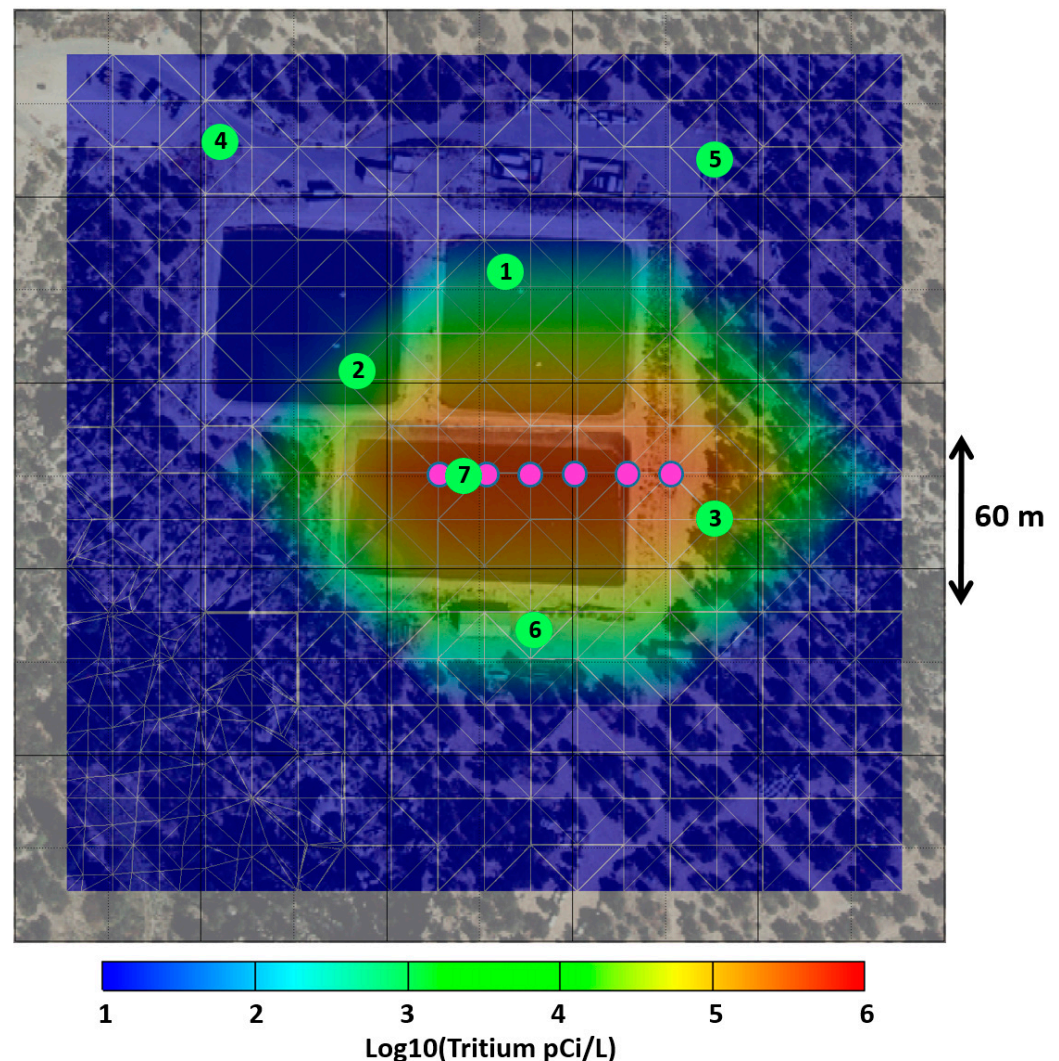


Figure 7. Image of the surface impoundments before they were removed. The numerical grid is overlain on the photo. The color contours are the simulated tritium plume at 2088 m elevation for the bounding case. The six pink dots show the location of the simulated leakage (injection) along the unlined drainage ditch. The green circles are the locations of Boreholes 1–7 drilled in 2002.

The total simulated leakage of tritium activity is 31.6 Ci. This likely represents a small fraction of the total tritium that flowed into the impoundments, because much of the effluent evaporated before reaching the unlined drainage ditch. Based on the simulated volume fraction of discharge that infiltrated in the ditch (7%), the results imply that effluent flowing past the drainage ditch could have carried as many as 450 Ci beyond the mesa edge. Fortunately, much of this tritium would have evaporated along the flow path before reaching Los Alamos Canyon.

3.2.1. Tritium

The simulated tritium concentrations with depth at the location of Borehole 7 and for the year 2002, are compared to the set of 2002 borehole tritium data (converted to pore water concentration (pCi/L)) for the seven investigation boreholes in Figure 8. Simulation results are interpolated to the same locations as the measured Borehole 7 data using a quad-linear interpolation scheme with the nearest four points from the same elevation. The simulation captures the general character of the measured Borehole 7 tritium data. The only apparent difference is that the measurements show little tritium moving below the Qbt1v-Qbt1g contact, while the simulation over-predicts the depth of the transport. This

difference is likely the result of incomplete knowledge of the surface release history, with the simulated release history having more water reaching depth than occurred at the site.

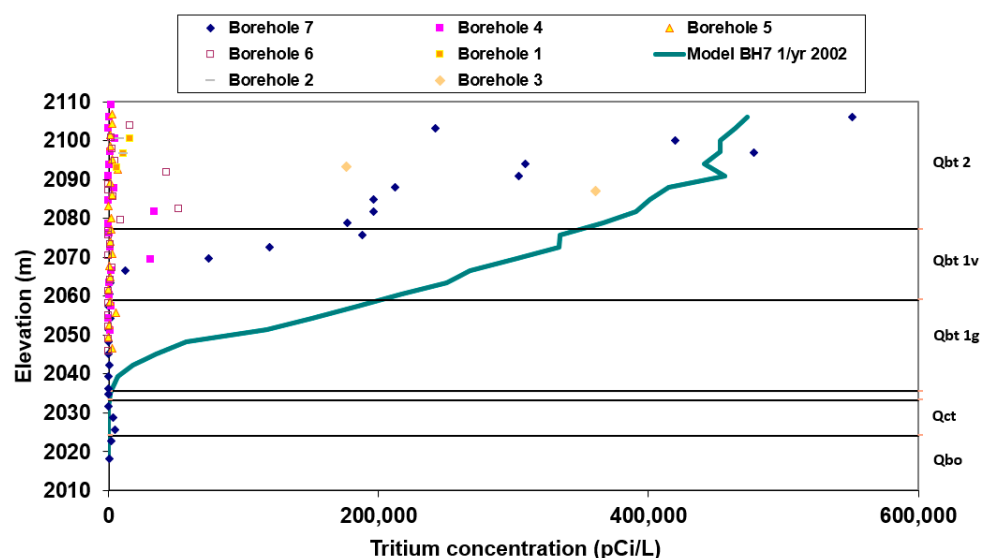


Figure 8. Simulated (at Borehole 7 location) and measured tritium concentrations for the year 2002.

Data from Boreholes 4, 5, and 6 (Figures 7 and 8) support the conceptual model for primary leaking along the unlined ditch because tritium was measured to be quite low on the perimeter of the impoundments, especially to the north. Data from Boreholes 1 and 2 (Figures 7 and 8) also support assumptions that the most likely location of major tritiated water migration to depth occurred along the unlined drainage ditch. These boreholes indicate that there was no significant leakage of tritiated water across the clay liner in the northern impoundments.

3.2.2. Saturation

As a further examination of the simulation fidelity, the bounding case, simulated saturation profile was compared to the Borehole 7 saturation data from Table 2 (Figure 9). For comparison purposes, saturation data from Mesita del Buey [26] are also represented as the light blue shaded areas in Figure 9. Mesita del Buey is a similar mesa located south of the study site but was not impacted by large volumes of water disposal, and thus represents a more natural condition. The background simulation used as the initial saturation state for the tritium analysis is also shown in Figure 9. The initial saturation in Qbt2 is at the high end of the background compared to Mesita del Buey. Saturations within Qbt1g are within the drier part of the Mesita del Buey field. In the Qct and Qbo units, the initial saturation is drier than in Mesita del Buey. However, the Borehole 7 data indicate that conditions are drier in these units than at Mesita del Buey. A comparison of the 2002 data with the saturation ranges shows increased liquid saturation from the surface to an elevation of 2065 m in Borehole 7. Although saturation in Borehole 7 in the lower part of Unit Qbt1g appears to be elevated above the background, the tritium values associated with this water are relatively low and suggest that the source of water was not from the higher-concentration southern impoundment. Major ion analysis indicates that an alternate source of infiltration is likely to have occurred before the tritium release.

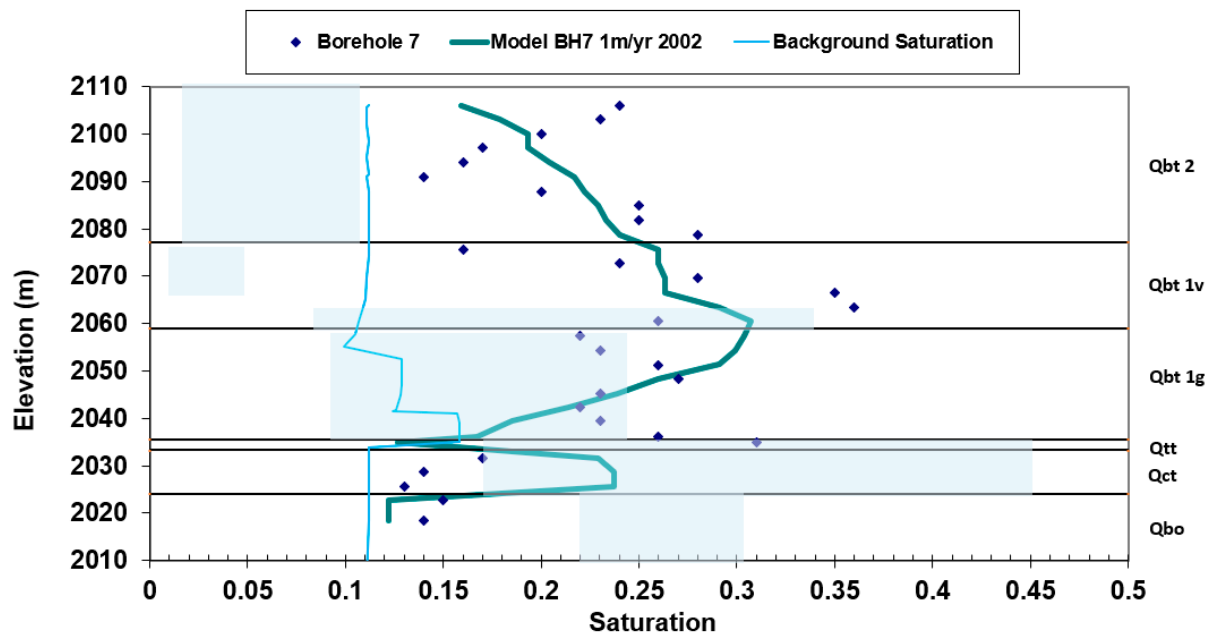


Figure 9. Simulations of saturation compared to site data for Borehole 7. The transparent blue shaded areas are 1 sigma saturation ranges from data presented by Birdsell et al. (2000) representing saturation ranges for a nearby mesa unimpacted by surface discharges.

4. Discussion

4.1. Implications of the Anion Profiles

One of the main objectives of this study was to determine what portion of the site was affected by leakage from the surface releases at TA-53. All the anion profiles from Borehole 7, except for those for nitrate and nitrite, have maximum concentrations and bulge-shaped profiles in the upper 45 m of the vadose zone (primarily in Qbt2 and the top of Qbt1v) (Figures 4 and 5). The anion profiles with bulges above 45 m are not identical in appearance, which may be related to variations in anion concentrations in the discharge waters with time, and/or variations in natural background concentrations. Nevertheless, the fact that six of the eight profiles have bulges/maximum concentrations in the same stratigraphic interval suggests that much of the impact of surface discharges near Borehole 7 are limited to approximately the upper 45 m of the vadose zone.

4.2. Implications of the $\delta^{18}\text{O}$ and $\delta^2\text{H}$ Profiles

The $\delta^{18}\text{O}$ and $\delta^2\text{H}$ stable isotope profiles from Borehole 7 show a distinct zone of higher isotopic composition that spans the same depth interval as the anion profile bulges (3- to about 45-m) (Figure 6). Thus, the isotope data also suggest that much of the impact of infiltrating impoundment water near Borehole 7 was limited to the upper 45 m of the vadose zone (elevations of 2110 m to 2065 m). The $\delta^{18}\text{O}$ values in this zone are approximately -3 to -2‰ and the $\delta^2\text{H}$ values are approximately -40 to -45‰ . These values are indicative of evaporation that would have been prevalent in the ditch and impoundments (during evaporation, the isotopic composition of the remaining water increases, i.e., becomes less negative). Though the change in isotopic values is abrupt at approximately 45 m, the data suggest there may have been some deeper leakage because the isotopic values have a smooth transition to more negative values below 45 m. A comparison of the $\delta^{18}\text{O}$ stable isotope values to the Borehole 7 tritium profile (Figure 10) also indicates that most impacts were limited to the upper 45 m near Borehole 7. Tritium concentrations are highest in the upper 45 m zone, and this matches the zone of highest stable isotope values and highest anion concentrations quite well.

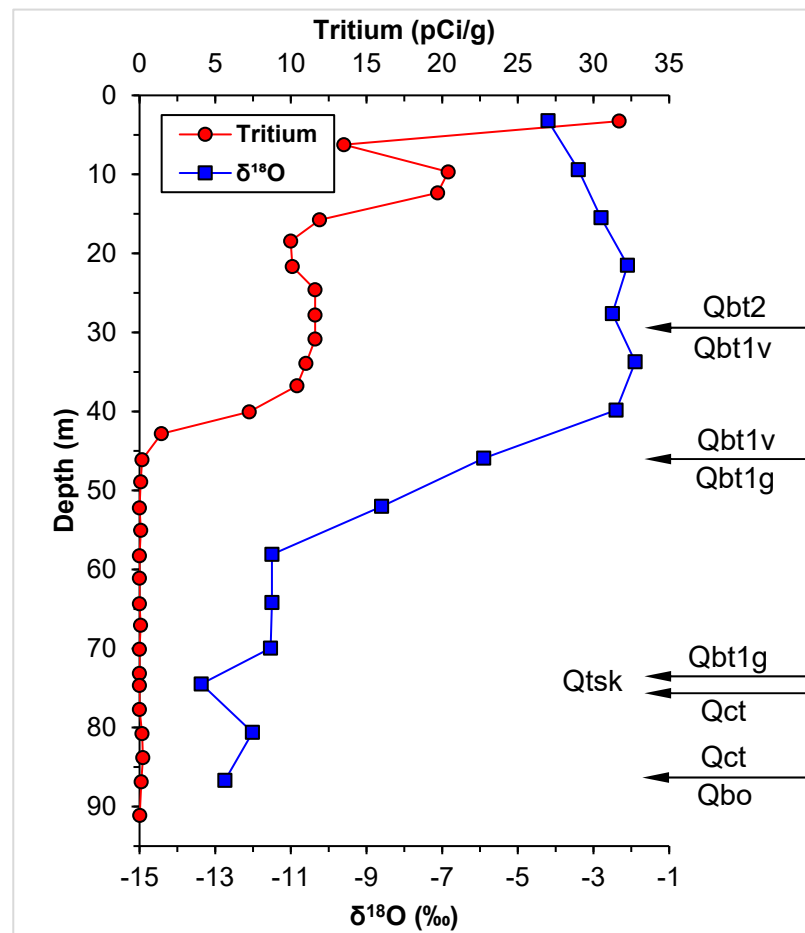


Figure 10. Comparison of $\delta^{18}\text{O}$ and tritium profiles in Borehole 7, TA-53.

4.3. Implications of the Nitrate, Nitrite, $\delta^{15}\text{N}$, and Tritium Data

Nitrate is sometimes found in semiarid vadose zones at concentrations equal to or greater than that observed in Borehole 7, including beneath other Los Alamos area mesas [17]. Thus, it is possible that the nitrate observed is from a natural source. However, there is strong evidence that some of, and perhaps a large fraction of, the nitrate inventory encountered in Borehole 7 (Figure 11) is not from natural sources. One piece of evidence is that the nitrate profile does not match the other anion profiles. Another reason is that the highest nitrate in Borehole 7 is associated with elevated water contents. Walvoord et al. [17] show that under natural conditions, high nitrate concentrations tend to be correlated with high concentrations of other anions such as chloride. In addition, the high natural nitrate concentrations at Mesita del Buey described in Walvoord et al. [17] were in low water content zones.

In addition, the water content profile in Figure 12 is unusual. If there was substantial and relatively continuous leakage from the ditch, one might expect elevated water content from the near-surface down to the point where enhanced percolation ceased. However, the Borehole 7 profile has a zone of elevated water content (some samples are $>10\%$) between approximately 30- and 80-m that is sandwiched between shallow and deep zones with water contents that are relatively low ($<7\%$). This kind of profile might form if there was a temporal change in the percolation of water such as variations in the amount of water flowing in the ditch.

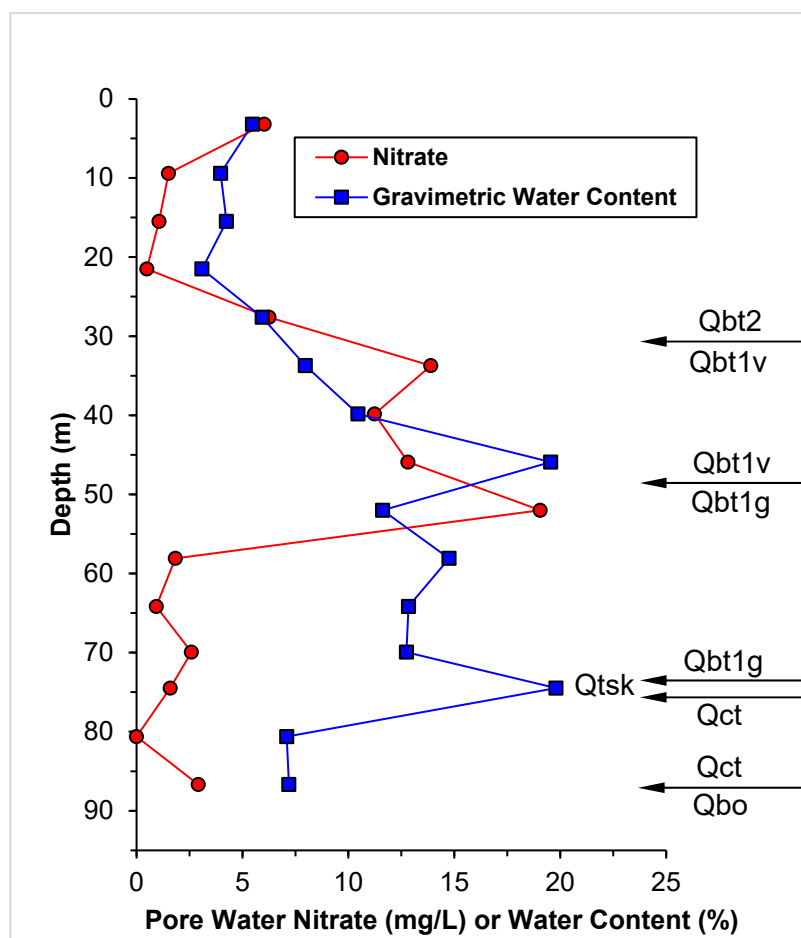


Figure 11. Comparison of Borehole 7 nitrate and gravimetric water content values.

The association of nitrate with the water content bulge suggests a sanitary waste component to the water in the elevated water content zone. The northern impoundment received sanitary waste until 1992 and the southern impoundment received sanitary waste from 1985 to 1989 [21,22]. The fact that there were nitrite detections in nearly half of the Borehole 7 samples also suggests a sanitary source (although the nitrite profile does not mimic the nitrate profile). Another factor that suggests a sanitary source for the nitrate and elevated water content is the Borehole 7 tritium profile (Figure 12). If the elevated water content and nitrate were largely derived from impoundment waters while tritium effluent was released, one would expect to see collocated elevated tritium concentrations; however, this is not the case. Instead, there is no tritium associated with nitrate below 45 m and this is where the maximum nitrate concentration was observed. If the source was mainly from sanitary waste, tritium would not be expected. This suggests that a sanitary nitrate source preceded the tritium effluent source to the impoundments. There is a region where the nitrate and tritium bulges overlap (about 30 m depth), which could result from commingling of the two sources.

The final piece of evidence supporting a sanitary waste source are the $\delta^{15}\text{N}$ results (Table 3). Nitrogen isotope values between approximately 10 and 20‰ are strongly indicative of sewage/sanitary waste [11,13]; eight of the ten samples fall within this range. A comparison of the $\delta^{15}\text{N}$ and nitrate profiles (Figure 13) show good, but not perfect, correlation between elevated nitrate concentrations and high $\delta^{15}\text{N}$ values, particularly at depths less than 45 m.

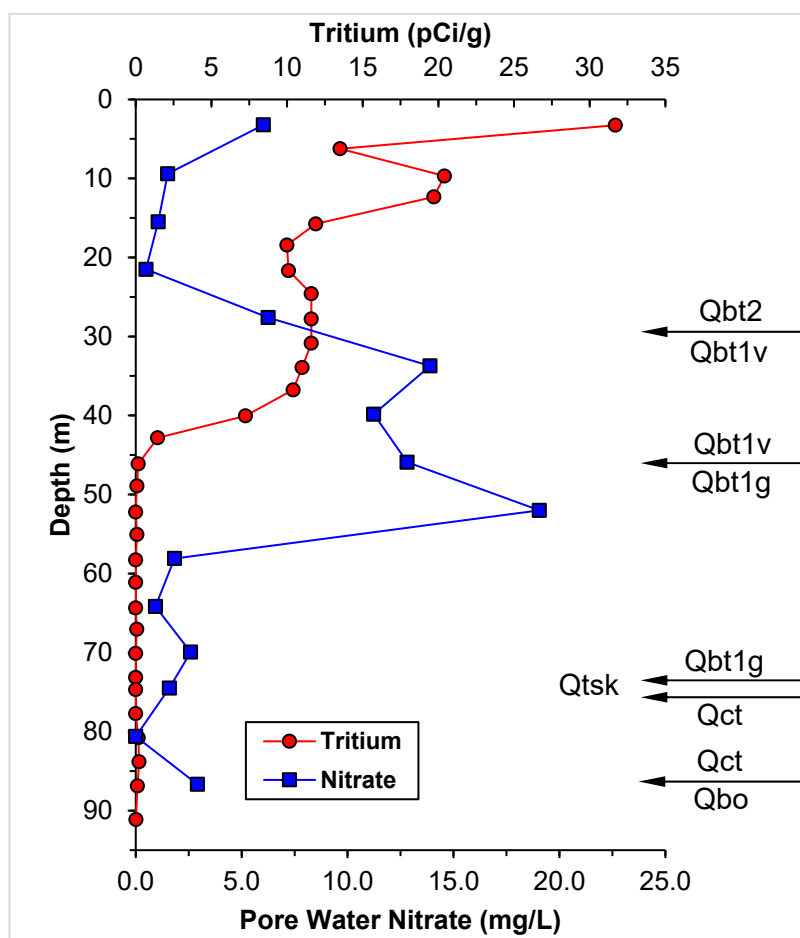


Figure 12. Comparison of nitrate and tritium profiles in Borehole 7.

4.4. Implications for Long-Term Risk of Tritium

The bounding case simulation was used to predict long-term tritium risk to the regional groundwater aquifer beneath the site. The numerical model was run from 1977 to 1992 with an infiltration flux of 1 m³ per m² per year over an area of 1394 m² representing the unlined drainage ditch. This area is shown as the pink nodes in Figure 7. Another 85 years of post-leakage drainage was then simulated to predict plume evolution following remediation. The infiltration flux for this latter period was 1 mm/year (1 L per square meter per year), the same as the flux applied over the other portions of the upper boundary. Maximum tritium concentrations drop rapidly during the 85 years of drainage as shown in Figure 14. By the simulated year 2070, all pore water concentrations in the plume drop below the EPA MCL of 20,000 pCi/L [7,8], and the tritium plume remains in the upper 100 m of the mesa. The regional aquifer at the site is at a depth of greater than 300 m. Therefore, these simulations indicate that the tritium plume will not pose a risk to groundwater because of a long travel time coupled with a short half-life. At longer times, the concentrations will decrease even further due to radioactive decay.

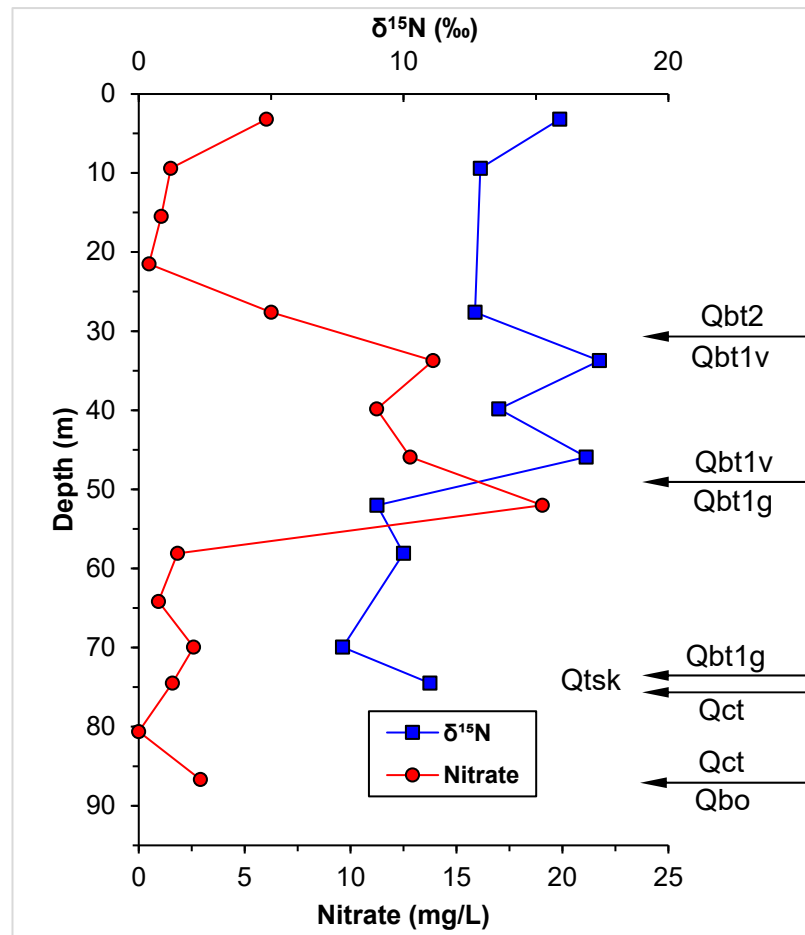


Figure 13. Comparison of $\delta^{15}\text{N}$ and nitrate profiles in Borehole 7.

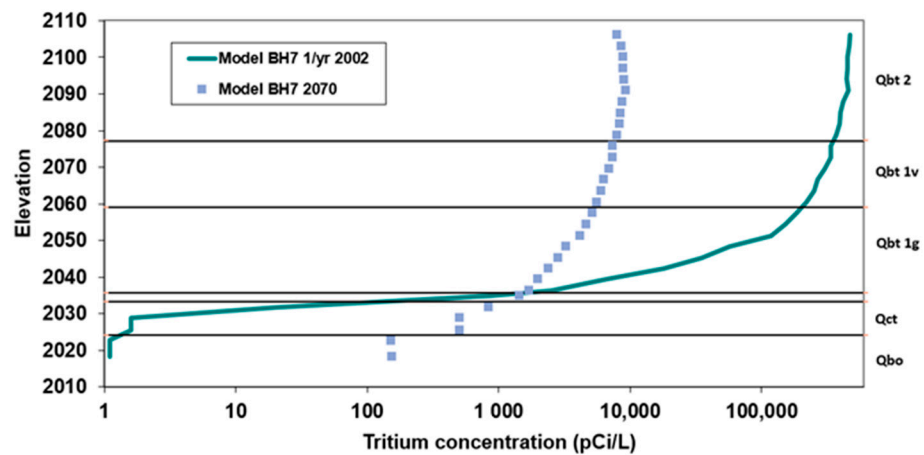


Figure 14. Simulated tritium concentrations vs. depth for the years 2002 and 2070.

The simulated migration of the water pulse is shown in Figure 15, where increased saturation drains downward from the upper 50 m of the profile in 2070, returning nearly to a background value at the land surface. The water from the upper section redistributes downward to units Qbt1g and Qct. The model predicts very little migration below the Qct, although slightly increased saturation in the Otowi member (Qbo) can be seen.

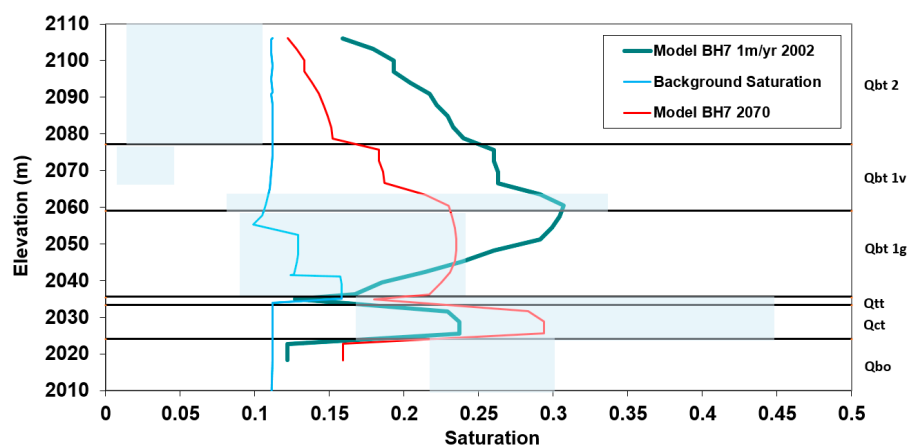


Figure 15. Simulated saturations versus depth for the background flow field and at years 2002 and 2070.

This set of simulations thus shows the power of radioactive decay for attenuating the tritium plume at TA-53. The ability of the unsaturated tuff at this site to redistribute water laterally also plays an important role in limiting the vertical extent of migration.

5. Conclusions

Analyses of the anion, stable isotope, and tritium data from Borehole 7 at the TA-53 surface impoundments suggest infiltration from the ditch or through impoundment leakage was primarily limited to the upper approximately 45 m of the vadose zone. The various data types, except for the nitrate and nitrite data, show profiles that are consistent with percolation of ditch water above approximately 45-m depth. This result seems reasonable because the Hypalon™ (rubber polymer) liner deployed in the southern impoundment should have limited the amount of downward water movement, and because water contents in the upper part of the vadose zone are low (typically <7%), which suggests not much water was moving into the vadose zone.

The nitrate, nitrite, $\delta^{15}\text{N}$, and water content data suggest an additional release source that preceded the main tritium releases and appears to have affected the vadose zone deeper than tritium. The nitrate, nitrite, $\delta^{15}\text{N}$, and water content data strongly suggest that this earlier source may be largely derived from sanitary waste that has percolated below the ditch. This interpretation is based on the lack of tritium and other anions at depths greater than 45 m, that nitrate and nitrite are commonly associated with sanitary waste, the isotopic composition of the nitrate, and that sanitary waste was released over many years at the site.

A tritium transport simulation, calibrated to the vertical extent of observed transport, was used to create a prediction of plume behavior to the year 2077. The combination of a relatively rapid radioactive decay (12.3-year half-life) and low liquid migration rates to depth (due to removal of the surface impoundments and high capillary forces in the relatively dry subsurface volcanic tuffs) provide a supportive environment for natural attenuation of the tritium plume. Tritium pore water concentrations in 2077 are predicted to fall well below the EPA drinking water MCL (<20,000 pCi/L), and the plume is predicted to remain in the vadose zone at a minimum of 200 m from the regional water table.

Dryland areas have been utilized for tritium disposal and are subject to other kinds of releases for many years because of high evapotranspiration rates, generally low subsurface moisture conditions, and deep groundwater. The results provide an additional confirmation that tritium transport in arid and semi-arid environments can be described using standard theory [6,9], with our work expanding the demonstrated usefulness of tritium transport simulations to situations where ponding in source regions drives flow to depth.

Author Contributions: Conceptualization, K.H.B., P.H.S. and B.D.N.; methodology, P.H.S., M.O.G. and B.D.N.; software, P.H.S. and T.A.M.; validation, P.H.S., E.C.K. and T.A.M.; formal analysis, B.D.N. and P.H.S.; data curation, M.O.G., B.D.N. and E.C.K.; writing—original draft preparation, P.H.S., K.H.B. and B.D.N.; writing—review and editing, P.H.S., K.H.B., B.D.N., J.M.H. and E.C.K.; visualization, B.D.N., P.H.S. and T.A.M.; supervision, P.H.S. and B.D.N.; project administration, P.H.S.; funding acquisition, P.H.S. All authors have read and agreed to the published version of the manuscript.

Funding: Funding for this work was provided by the United States Department of Energy’s Office of Environmental Management. Los Alamos Environmental Management provided technical support. This work was performed by the Los Alamos National Laboratory which is operated by Triad National Security for the National Nuclear Security Administration of the USDOE (Contract no. 89233218CNA000001) The United States Government retains and the publisher, by accepting this work for publication, acknowledges that the United States Government retains a nonexclusive, paid-up, irrevocable, worldwide license to publish or reproduce this work or allow others to do so for the United States Government purposes.

Institutional Review Board Statement: Not applicable.

Informed Consent Statement: Not applicable.

Data Availability Statement: Data are provided in the tables in the paper.

Acknowledgments: We wish to thank Andrew Campbell for providing the stable isotope analyses, and Jace Koger for his editorial assistance.

Conflicts of Interest: The authors declare no conflict of interest.

References

1. Newman, B.D.; Breshears, D.D.; Gard, M.O. Evapotranspiration partitioning in a semiarid woodland: Ecohydrologic heterogeneity and connectivity of vegetation patches. *Vadose Zone J.* **2010**, *9*, 561–572. [CrossRef]
2. Phillips, F.M. Environmental tracers for water movement in desert soils of the American Southwest. *Soil Sci. Soc. Am. J.* **1994**, *58*, 15–24. [CrossRef]
3. Aggarwal, P.K.; Gat, J.R.; Froehlich, K.F.O. *Isotopes in the Water Cycle, Past, Present, and Future of a Developing Science*; International Atomic Energy Agency (IAEA): Vienna, Austria, 2005; ISBN 10 1-4020-3010-X (HB).
4. Cauquoin, A.; Jean-Baptiste, P.; Risi, C.; Fourre, E.; Stenni, B.; Landais, A. The global distribution of natural tritium in precipitation simulated with an Atmospheric General Circulation Model and comparison with observations. *Earth Planet. Sci. Lett.* **2015**, *427*, 160–170. [CrossRef]
5. Maxwell, R.M.; Tompson, A.F.B.; Kollet, S. A serendipitous, long-term infiltration experiment: Water and tritium circulation beneath the CAMBRIC trench at the Nevada Test Site. *J. Cont. Hydrol.* **2009**, *108*, 12–28. [CrossRef]
6. Maples, S.R.; Andraski, B.J.; Stonestrom, D.A.; Cooper, C.A.; Pohll, G.M.; Michel, R.L. Tritium plume dynamics in the shallow unsaturated zone in an arid environment. *Vadose Zone J.* **2013**, *12*, 4. [CrossRef]
7. EPA. Interim Primary Drinking Water Regulations: Proposed Maximum Contaminant Levels for Radioactivity. *Fed. Regist.* **1975**, *40*, 34324–34328.
8. EPA. Drinking Water Regulations: Radionuclides. *Fed. Regist.* **1976**, *41*, 28402–28409.
9. Garcia, A.; Andraski, B.J.; Stonestrom, D.A.; Cooper, C.A.; Johnson, M.J.; Michel, R.L.; Wheatcraft, S.W. Transport of tritium contamination to the atmosphere in an arid environment. *Vadose Zone J.* **2009**, *8*, 450–461. [CrossRef]
10. Hodges, R.A.; Cooper, C.A.; Falta, R.W. Modeling of flow and transport by production of hydrofracture-stimulated gas wells near the Rulison nuclear test. *Transp. Porous Media* **2015**, *108*, 23–42. [CrossRef]
11. Clark, I.D.; Fritz, P. *Environmental Isotopes in Hydrogeology*; Lewis Publishers: Boca Raton, FL, USA, 1997; p. 149.
12. Cappa, C.D.; Hendricks, M.B.; DePaolo, D.J.; Cohen, R.C. Isotopic fractionation of water during evaporation. *J. Geophys. Res.* **2003**, *108*, D16. [CrossRef]
13. *Isotope Tracers in Catchment Hydrology*; Kendall, C.; McDonnell, J. (Eds.) Elsevier: Amsterdam, The Netherlands, 1998; p. 839.
14. Allison, G.B.; Barnes, C.J.; Hughes, M.W. The distribution of deuterium and ¹⁸O in dry soils: 2. Experimental. *J. Hydrol.* **1983**, *64*, 377–397. [CrossRef]
15. Barnes, C.J.; Allison, G.B. The distribution of deuterium and ¹⁸O in dry soils: 1. Theory. *J. Hydrol.* **1983**, *64*, 141–156. [CrossRef]
16. Newman, B.D.; Campbell, A.R.; Wilcox, B.P. Tracer-based studies of soil water movement in semi-arid forests of New Mexico. *J. Hydrol.* **1997**, *196*, 251–270. [CrossRef]
17. Walvoord, M.A.; Phillips, F.M.; Stonestrom, D.A.; Evans, R.D.; Hartsough, P.C.; Newman, B.D.; Striegl, R.G. A Reservoir of Nitrate Beneath Desert Soils. *Science* **2003**, *302*, 1021–1024. [CrossRef] [PubMed]
18. LANSCE. Available online: <https://lansce.lanl.gov/facilities/linac.php> (accessed on 19 July 2022).

19. Newman, B.D.; Robinson, B.A. The hydrogeology of Los Alamos National Laboratory: Site history and overview of vadose zone and groundwater contamination issues. *Vadose Zone J.* **2005**, *4*, 614–619. [[CrossRef](#)]
20. Broxton, D.E.; Vaniman, D.T. Geologic Framework of a Groundwater System on the Margin of a Rift Basin, Pajarito Plateau, North-Central New Mexico. *Vadose Zone J.* **2005**, *4*, 522–550. [[CrossRef](#)]
21. Los Alamos National Laboratory. *RFI Work Plan and SAP for Potential Release Sites 53-002(a), 53-002(b), and Associated Piping and Drainages at TA-53*; Los Alamos National Laboratory Report, LA-UR-98-2547; Los Alamos National Laboratory: Los Alamos, NM, USA, 1998.
22. Los Alamos National Laboratory. *Addendum II to RFI Work Plan and SAP for Potential Release Sites 53-002(a), 53-002(b), and Associated Piping and Drainages at TA-53*; Los Alamos National Laboratory report, LA-UR-02, 4013; Los Alamos National Laboratory: Los Alamos, NM, USA, 2002.
23. Los Alamos National Laboratory. *Investigation and Remediation Report for Consolidated SWMU 53-002(a)-99, Inactive Wastewater Impoundments, and AOC 53-008, Storage Area*; at Technical Area 53, Revision 1, Los Alamos National Laboratory report, LA-UR-05, 6373; Los Alamos National Laboratory: Los Alamos, NM, USA, 2005.
24. Stauffer, P.H.; Levitt, D.G.; Miller, T.A.; Jordan, A.; Chu, S.; Dash, Z. *Groundwater Pathway Model for the Los Alamos National Laboratory Technical Area 21, Material Disposal Area T*; Los Alamos National Laboratory report, LA-UR-17-21054; Los Alamos National Laboratory: Los Alamos, NM, USA, 2017.
25. Stauffer, P.H.; Birdsell, K.H.; Dai, Z.; Levitt, D.; Atchley, A.; Pawar, R.J.; Chu, S.P.; French, S.B. *Simulated Impacts of Water Introduced into Pits 37 and 38 at Technical Area 54, Area G*; Los Alamos National Laboratory report, LA-UR-16-29480; Los Alamos National Laboratory: Los Alamos, NM, USA, 2017.
26. Birdsell, K.H.; Wolfsberg, A.V.; Hollis, D.; Cherry, T.A.; Bower, K.M. Groundwater Flow and Radionuclide Transport Calculations for a Performance assessment of a Low-Level Waste Site. *J. Contam. Hydrol.* **2000**, *46*, 99–129. [[CrossRef](#)]
27. Turin, H.J.; Rosenberg, N. A Conceptual Model for Flow in the Vadose Zone Beneath Finger Mesas of the Pajarito Plateau. In Proceedings of the New Mexico Geological Society 47th Annual Field Conference, Socorro, NM, USA, 25–28 September 1996; Goff, F., Kues, B.S., Rogers, M.A., McFadden, L.D., Gardner, J.N., Eds.; NM Bureau of Geology & Mineral Resources: Socorro, NM, USA, 1996. 484p.
28. Birdsell, K.H.; Newman, B.D.; Broxton, D.E.; Robinson, B.A. Conceptual models of vadose zone flow and transport beneath the Pajarito Plateau, Los Alamos, NM. *Vadose Zone J.* **2005**, *4*, 620–636. [[CrossRef](#)]
29. Robinson, B.A.; McLin, S.G.; Viswanathan, H.S. Hydrologic Behavior of Unsaturated, Fractured Tuff: Interpretation and Modeling of a Wellbore Injection Test. *Vadose Zone J.* **2005**, *4*, 694–707. [[CrossRef](#)]
30. Cooper, C.A.; Chapman, J.B. *Radionuclide Migration at the Gasbuggy Underground Nuclear Test Site*; LMS/GSB/S13226, DRI Report No. 41262; DRI: Alexandria, VA, USA, 2015.
31. Knight, J.H. An Improved Approximation of Spherical Diffusion of Tritium in Relatively Dry Soil. *Water Resour.* **1996**, *32*, 349–354. [[CrossRef](#)]
32. Smiles, D.E.; Gardner, W.R.; Shultz, R.K. Diffusion of Tritium in Arid Disposal Sites. *Water Resour. Res.* **1995**, *31*, 1438–1488. [[CrossRef](#)]
33. Zyvoloski, G.A.; Robinson, B.A.; Dash, Z.V.; Trease, L.L. *Summary of the Models and Methods for the FEHM Application—A Finite-Element Heat- and Mass-Transfer Code*; Los Alamos National Laboratory report LA-13307-MS; Los Alamos National Laboratory: Los Alamos, NM, USA, 1997.
34. Zyvoloski, G.A.; Robinson, B.A.; Dash, Z.V.; Kelkar, S.; Viswanathan, H.S.; Pawar, R.J.; Stauffer, P.H.; Miller, T.A.; Chu, S.P. *Software Users Manual (UM) for the FEHM Application Version 3.1–3.X.*; Los Alamos National Laboratory Report, LA-UR-12-24493; Los Alamos National Laboratory: Los Alamos, NM, USA, 2015.
35. Available online: <https://fehm.lanl.gov/> (accessed on 19 July 2022).
36. Rogers, D.B.; Gallaher, B.M. *The Unsaturated Hydraulic Characteristics of the Bandelier Tuff*; Los Alamos National Laboratory Report, LA-12968-MS; Los Alamos National Laboratory: Los Alamos, NM, USA, 1995.
37. Shurbaji, A.R.; Campbell, A.R. A study of evaporation and recharge in desert soils using environmental tracers, New Mexico, USA. *Environ. Geol.* **1997**, *29*, 147–151. [[CrossRef](#)]
38. Socki, R.A.; Karlsson, H.R.; Gibson, E.K. Extraction technique for determination of oxygen-18 in water using preevacuated glass vials. *Anal. Chem.* **1992**, *64*, 829–831. [[CrossRef](#)]
39. Kendall, C.; Coplen, T.B. Multisample conversion of water to hydrogen by zinc for stable isotope determination. *Anal. Chem.* **1985**, *57*, 1437–1446. [[CrossRef](#)]
40. Chang, C.C.Y.; Langston, J.; Riggs, M.; Campbell, D.H.; Silva, S.R.; Kendall, C. A method for nitrate collection for delta N-15 and delta O-18 analysis from waters with low nitrate concentrations. *Can. J. Fish. Aquat. Sci.* **1999**, *56*, 1856–1864. [[CrossRef](#)]
41. Silva, S.R.; Kendall, C.; Wilkison, D.H.; Ziegler, A.C.; Chang, C.C.Y.; Avanzino, R.J. A new method for collection of nitrate from fresh water and the analysis of nitrogen and oxygen isotope ratios. *J. Hydrol.* **2000**, *228*, 22–36. [[CrossRef](#)]
42. Stauffer, P.H. *Tritium Transport Beneath Surface Impoundments at TA-53 Modeling and Analysis in Support of Data Needs*; Los Alamos National Laboratory Report, LA-UR-02-5321; Los Alamos National Laboratory: Los Alamos, NM, USA, 2002.
43. Viswanathan, H.S.; Robinson, B.A.; Valocchi, A.J.; Triay, I.R. A reactive transport model of neptunium migration from the potential repository at Yucca Mountain. *J. Hydrol.* **1998**, *209*, 251–280. [[CrossRef](#)]

44. Stauffer, P.H.; Vrugt, J.A.; Turin, H.J.; Gable, C.W.; Soll, W.E. Untangling diffusion from advection in unsaturated porous media: Experimental data, modeling, and parameter uncertainty assessment. *Vadose Zone J.* **2009**, *8*, 510–522. [[CrossRef](#)]
45. Robinson, B.A.; Chu, S.; Lu, Z. Simulation of Radionuclide Transport through Unsaturated, Fractured Rock: Application to Yucca Mountain, Nevada. *Vadose Zone J.* **2012**, *11*, 15. [[CrossRef](#)]
46. Stauffer, P.H.; Birdsell, K.H.; Witkowski, M.S.; Hopkins, J.K. Vadose Zone Transport of 1,1,1-Trichloroethane: Conceptual Model Validation through Numerical Simulation. *Vadose Zone J.* **2005**, *4*, 760–773. [[CrossRef](#)]
47. Neeper, D.A.; Stauffer, P.H. Transport by oscillatory flow in soils with kinetic mass transfer I. *Theory Vadose Zone J.* **2012**, *11*, 14. [[CrossRef](#)]
48. Neeper, D.A.; Stauffer, P.H. Transport by oscillatory flow in soils with kinetic mass transfer II. Field Experiment. *Vadose Zone J.* **2012**, *11*, 14. [[CrossRef](#)]
49. Kwicklis, E.M.; Wolfsberg, A.V.; Stauffer, P.H.; Walvroord, M.A.; Sully, M.J. Multiphase Multicomponent Parameter Estimation for Liquid and Vapor Flu. *Vadose Zone J.* **2006**, *5*, 934–950. [[CrossRef](#)]
50. LaGrit. Los Alamos Grid Toolbox. Available online: <https://lagrit.lanl.gov/> (accessed on 19 July 2022).
51. Carey, B.; Cole, G.; Lewis, C.; Tsai, F.; Warren, R.; WoldeGabriel, G. *Revised Site-Wide-Geologic Model for Los Alamos National Laboratory (FY99)*; Los Alamos National Laboratory Report LA-UR-00-2056; Los Alamos National Laboratory: Los Alamos, NM, USA, 1999; p. 66782.
52. Miller, T.A.; Vessilnov, V.V.; Stauffer, P.H.; Birdsell, K.H.; Gable, C.W. Integration of Geologic Frameworks in Meshing and Setup of Computational Hydrogeologic Models, Pajarito Plateau, New Mexico. In *New Mexico Geological Society Guide Book 58th Field Conference, Geology of the Jemez Mountains Region III, USA, 2007*; New Mexico Bureau of Geology and Mine: Socorro, NM, USA, 2007.
53. Stauffer, P.H.; Rosenberg, N.D. Vapor phase transport at a hillside landfill. *Environ. Eng. Geosci.* **2000**, *6*, 71–84. [[CrossRef](#)]